

ANTI-PROTON–HYDROGEN ATOM COLLISION AT INTERMEDIATE ENERGY

Using a molecular-orbital close-coupling approach, the authors study ionization processes in antiproton–hydrogen atom collision and present visualizations of the electron densities' time development during the collision.

The study of dynamical aspects in ion–atom collision processes is important in atomic physics. It helps us fundamentally understand particle interactions and the corresponding dynamics for applications in many subfields, such as fusion sciences, astrophysics, and material sciences. Furthermore, it presents an interesting problem as the basic physics. Energetic collision of two particles can produce processes; for example, ion–atom collisions frequently produce elastic scattering, electronic excitation, charge transfer, and ionization. An accurate description of the electrons' behavior during the collision is essential to better understand the dynamics and precisely determine cross sections for these processes.

To investigate the collision dynamics in detail, we must observe how the electronic state varies as the incident ion nears the target atom. Be-

cause measuring various observables as a function of the collision time is difficult, numerical simulation of the collision process is the only way to “see” the instantaneous collision, so it has attracted much attention.^{1,2} The simulation study must also include effective visualization schemes.

We study the dynamics of ionization in antiproton–hydrogen collisions using a molecular-orbital close-coupling (MOCC) method.¹ We present the numerical result using a simulation technique to visualize the ionization and better understand the collision dynamics.

Antiproton–hydrogen collision

To illuminate the disparity between the amount of matter and antimatter in the universe (for more on antimatter, see the sidebar), researchers are conducting several projects—using various approaches—that attempt to differentiate ordinary hydrogen and antihydrogen (which comprises a positron and an antiproton).^{3–9}

Most calculations agree reasonably well with the experimental results¹⁰ at the high-energy region (above a few tens of kilo–electron volts) but—in our opinion—not the lower energy region (below a few tens of keV). Furthermore, physicists have not explored collision dynamics' details, such as the evolution time of charge den-

1521-9615/02/\$17.00 © 2002 IEEE

REIKO SUZUKI

Hitotsubashi University

HIROSHI SATO

Ochanomizu University

MINEO KIMURA

Yamaguchi University

sities, to better understand this collision's essential physics.

So, we investigated the collision dynamics of ionization stemming from antiproton–hydrogen collisions at energies below 50 keV. In this energy region, the colliding partners' relative velocity is much smaller than the electron's velocity, so we can safely assume that the particles form a quasimolecule during collision. Therefore, we can describe the collision system's electronic state in terms of molecular states, which is known as *molecular-orbital representation*. Additionally, we can use the *semiclassical approximation*, wherein we treat the baryon motion classically but the electron quantum-mechanically. We employed an MOCC method¹ in the semiclassical formulation to study the scattering dynamics.

First, we determine adiabatic potentials using a configuration interaction method with Sturmian-type wave functions as expansion bases, as we explain later. Consequently, many electronic states with positive eigenenergies appear, which probably correspond to ionized states. By including these positive-energy states in a discretized manner in our CC formulation, we can investigate ionization processes resulting from the collision.

Theoretical model

You can find details of the MOCC's basic formulation in the report by Ayako Watanabe and her colleagues.¹¹ We consider the antiproton–hydrogen collision system in the collision energy region from several electron volts per unit to several keV/u. Figure 1 shows colliding particles' coordinates.

The large disparity between the nuclear and electron masses makes it reasonable to approximate the nucleus's relative motion classically above a few tens of eV. We use an atomic unit system throughout this article unless otherwise stated ($e = m = \hbar = 1$, where e is the electronic charge, m the electronic mass, and \hbar the Planck constant/ 2π). The relative coordinate is given by Newton's equation

$$M \frac{d^2 \mathbf{R}(t)}{dt^2} = -\nabla V(\mathbf{R}), \quad (1)$$

where M is the reduced mass of two nuclei. We can solve the equation of motion (Equation 1) for the given impact parameter \mathbf{b} and initial velocity \mathbf{v}_0 to determine the relative coordinate's time dependence. We use a straight-line trajec-

Antiparticles

Because of technological advances in experimental methods in the last decade, various types of particle beams are readily available. Using these beams, we can conduct different collision experiments to investigate spectroscopic and dynamical quantities of atomic and molecular species. Until now, these particle beams comprised mostly electrons, ions, neutral atoms, and molecules. Recently, antiparticles (such as positrons and antiprotons), which cannot exist as stable particles in our natural environment, have become available for atomic collision experiments. Using the antiproton beam, especially, opens up a new physics field.

Physicists believe a particle and its antiparticle have the same physical properties, such as mass, but the opposite charge. However, only a small fraction of antimatter is known to exist in nature, a fact that scientists have been unable to explain. The suspected reason is CP asymmetry, first noted by James Cronin and Val Fitch. Recently, the European Center for Nuclear Research (CERN) produced cold antihydrogen atoms.¹ This research's ultimate goal will be to test the CPT theorem using this antihydrogen.

Reference

1. M. Amoretti et al., "Production and Detection of Cold Antihydrogen Atoms," *Nature*, advance online publication, 18 Sept. 2002; www.nature.com.

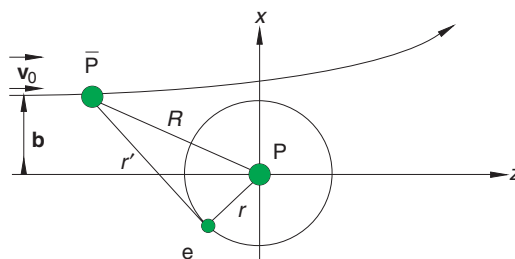


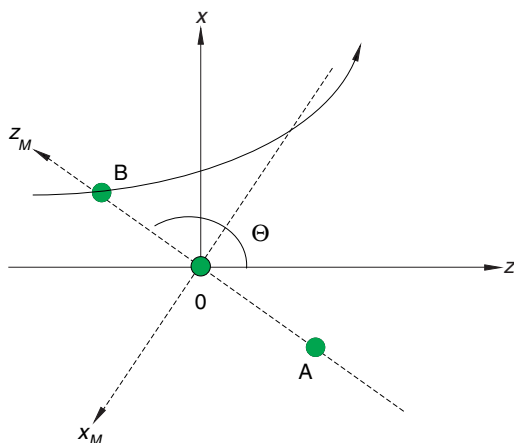
Figure 1. A model of antiproton–hydrogen atom collision. R , r , and r' denote the distance between the proton (P) and antiproton (P-bar), the electron (e) and proton, and the electron and antiproton, respectively. \mathbf{b} is the impact parameter, and \mathbf{v}_0 is the initial velocity.

tory for heavy particles because we believe it is a good description when the collision energy is larger than several tens of eV/u. The electron motion satisfies the Schrödinger equation

$$i \frac{\partial}{\partial t} \Psi(\mathbf{r}, t; \mathbf{R}(t)) = H_{el} \Psi(\mathbf{r}, t; \mathbf{R}(t)), \quad (2)$$

where H_{el} is the electronic Hamiltonian, and $\Psi(\mathbf{r}, t; \mathbf{R}(t))$ is the total scattering wave function.

Figure 2. The molecular coordinates.



The Hamiltonian is given by

$$H_{el} = -\frac{1}{2} \nabla^2 - \frac{1}{r} + \frac{1}{r'} - \frac{1}{R}. \quad (3)$$

Close-coupling method

In the close-coupling method,¹ we expand the total wave function Ψ in terms of known functions $\{\Psi_j\}$:

$$\begin{aligned} \Psi(\mathbf{r}, t; \mathbf{R}(t)) = & \sum_j c_j(t) \Psi_j(\mathbf{r}; \mathbf{R}(t)) \\ & \cdot \exp\left[-i \frac{1}{2} \frac{d\mathbf{R}(t)}{dt} \cdot \mathbf{r}\right] \\ & \cdot \exp\left[-i \int E_j(\mathbf{R}(t)) dt\right]. \end{aligned} \quad (4)$$

Here, $\exp\left[-i \frac{1}{2} \frac{d\mathbf{R}(t)}{dt} \cdot \mathbf{r}\right]$ represents the electron translation factor, which accounts for an electron moving together with moving nuclei.

At the low- to intermediate-energy region, we consider it appropriate to choose the electronic Hamiltonian's eigenfunctions $\{\Psi_j\}$ —that is, a molecular state within the Born-Oppenheimer approximation—as the basis of the expansion:

$$H_{el} \Psi_j(\mathbf{r}; \mathbf{R}) = E_j(\mathbf{R}) \Psi_j(\mathbf{r}; \mathbf{R}), \quad (5)$$

where Ψ_j satisfies an orthonormality condition

$$\int \Psi_i^*(\mathbf{r}; \mathbf{R}) \Psi_j(\mathbf{r}; \mathbf{R}) d\mathbf{r} = \delta_{ij}. \quad (6)$$

By substituting the expansion (Equation 4) into the Schrödinger equation (Equation 2), we derive a set of coupled equations in terms of the expansion coefficient $c_j(t)$ as follows:

$$\begin{aligned} i\dot{c}_i = & \frac{\mathbf{R}^2}{8} c_i \\ & -i \sum_j c_j \dot{\mathbf{R}} \cdot \langle \Psi_i | \nabla_R - \frac{1}{2} \nabla_r | \Psi_j \rangle \\ & \cdot \exp[-i \int (E_j - E_i) dt] \\ & - \sum_j \frac{1}{2} c_j \ddot{\mathbf{R}} \cdot \langle \Psi_i | \mathbf{r} | \Psi_j \rangle \\ & \cdot \exp[-i \int (E_j - E_i) dt]. \end{aligned} \quad (7)$$

We solve these coupled equations under the appropriate initial condition $\{c_j(-\infty)\}$.

Equation 7 clearly shows that if the relative speed $\dot{\mathbf{R}}$ is nonzero, then the transition between different states becomes possible. Because we assume the nucleus's relative speed is slow compared to that of orbital electrons, we ignore the term beyond the square of the relative speed and must only evaluate up to the second term.

Generally, it is convenient to represent the coupled equation in terms of the molecular coordinates. We use $\mathbf{i}, \mathbf{j}, \mathbf{k}$ —basic unit vectors—and M , a subscript, for the molecular coordinates. Figure 2 shows the molecular coordinate ($0 - x_M y_M z_M$) system.

Using the molecular coordinates, we can rewrite the second term in the coupled Equation 7 as

$$\begin{aligned} \dot{\mathbf{R}} \cdot \langle \Psi_i | \nabla_R - \frac{1}{2} \nabla_r | \Psi_j \rangle & = \dot{R} \cdot \langle \Psi_i | \frac{\partial}{\partial R} - \frac{1}{2} \frac{\partial}{\partial z_M} | \Psi_j \rangle \\ & - \dot{\Theta} \cdot \langle \Psi_i | i l_{yM} + \frac{1}{2} R \frac{\partial}{\partial x_M} | \Psi_j \rangle. \end{aligned} \quad (8)$$

In this equation, the first term is called a *radial coupling term* owing to the nuclei's radial motion, while the second term is a *rotational coupling term*, which arises from the molecular axis's rotation. From now on, we omit the subscript M from the notation because all our discussions are based on the molecular-coordinate framework. We derive the new form of the coupled equation:

$$\begin{aligned} i\dot{c}_i = & -i \sum_j c_j \cdot \left\{ \dot{R} \cdot \langle \Psi_i | \frac{\partial}{\partial R} - \frac{1}{2} \frac{\partial}{\partial z} | \Psi_j \rangle \right. \\ & \left. - \dot{\Theta} \cdot \langle \Psi_i | i l_y + \frac{1}{2} R \frac{\partial}{\partial x} | \Psi_j \rangle \right\} \\ & \cdot \exp[-i \int (E_j - E_i) dt]. \end{aligned} \quad (9)$$

Molecular orbitals

We describe the electronic wave function with a linear combination of basis function ψ :

$$\Psi_j(\mathbf{r}; \mathbf{R}) = \sum_i \alpha_i(\mathbf{R}) \psi_{n_i, l_i, m_i}(\mathbf{r}). \quad (10)$$

Because electrons and antiprotons have negative charges and, therefore, repel each other, we assume that the electron localizes around the proton. Therefore, the one-center expansion method should describe the electron distribution reasonably well. Sturmian functions¹ are regular solutions of the hydrogenic radial equation with a fixed alpha value, and as a result, we can simplify the general formulation using orthonormalized sturmian-type basis functions. So, we adopt the Sturmian-type basis function and expand it on the hydrogen atom:

$$\begin{aligned} \psi_{nlm}(\mathbf{R}) \\ = \alpha^{\frac{3}{2}} N_{nl} \cdot e^{-\frac{1}{2}\rho} \cdot \rho^l \cdot L_{n-l-1}^{2l+2}(\rho) Y_{lm}(\theta, \phi), \end{aligned} \quad (11)$$

where $\rho = \alpha r$, and α is a nonlinear variable parameter. $L_{n-l-1}^{2l+2}(\rho)$ is the Laguerre polynomial, which has the form

$$\begin{aligned} L_{n-l-1}^{2l+2}(\rho) \\ = \sum_{r=0}^{n-l-1} (-1)^r \frac{(n+l+1)!}{r!(2l+r+2)!(n-l-1-r)!} \rho^r. \end{aligned} \quad (12)$$

Here, $Y_{lm}(\theta, \phi)$ denotes the spherical harmonic.

Using the variable method,¹² we can derive the secular equation for the electronic Hamiltonian:

$$\det |H_{ij} - E_i| = 0. \quad (13)$$

We can solve this secular equation to obtain energies and wave functions.

To solve Equation 13, we must evaluate the matrix element of the electronic Hamiltonian (Equation 3):

$$\begin{aligned} H_{ij} = & \langle n_i, l_i, m_i | \left[-\frac{1}{2} \nabla^2 \right] | n_j, l_j, m_j \rangle \\ & - \langle n_i, l_i, m_i | \frac{1}{r} | n_j, l_j, m_j \rangle \\ & + \langle n_i, l_i, m_i | \frac{1}{r'} | n_j, l_j, m_j \rangle - \frac{1}{R} \delta_{ij}. \end{aligned} \quad (14)$$

In this equation, the first term

$$\langle n_i, l_i, m_i | \left[-\frac{1}{2} \nabla^2 \right] | n_j, l_j, m_j \rangle$$

represents the nuclear kinetic energy operator,

$$- \langle n_i, l_i, m_i | \frac{1}{r} | n_j, l_j, m_j \rangle$$

is the Coulomb interaction between the electron and nuclei, and

$$\langle n_i, l_i, m_i | \frac{1}{r'} | n_j, l_j, m_j \rangle$$

is the Coulomb repulsive interaction between the electron and antiproton.

The kinetic energy operator is

$$\begin{aligned} \langle n_i, l_i, m_i | \left[-\frac{1}{2} \nabla^2 \right] | n_j, l_j, m_j \rangle \\ = \frac{\alpha^2}{8} \delta_{ll'} \delta_{mm'} A \times (2l+k+k')! \\ \cdot [4l^2 + 6l - k^2 + k + 2kk' - k'^2 + k' + 2], \end{aligned} \quad (15)$$

where

$$\begin{aligned} A = N_{n_i l_i} N_{n_j l_j} \sum_{k=0}^{n-l-1} \frac{(-1)^k (n+l+1)!}{k!(2l+k+2)!(n-l-1-k)!} \\ \times \sum_{k'=0}^{n'-l-1} \frac{(-1)^{k'} (n'+l+1)!}{k'!(2l+k'+2)!(n'-l-1-k')!}. \end{aligned} \quad (16)$$

The Coulomb interaction between the electron and nuclei can be expressed as

$$\begin{aligned} \langle n_i, l_i, m_i | \frac{1}{r} | n_j, l_j, m_j \rangle \\ = \alpha \delta_{ll'} \delta_{mm'} A (2l+1+k+k')! \end{aligned} \quad (17)$$

We rewrite the Coulomb repulsive interaction between the electron and antiproton as

$$\begin{aligned} \langle n_i, l_i, m_i | \frac{1}{r'} | n_j, l_j, m_j \rangle \\ = \alpha A (-1)^m [(2l+1)(2l'+1)]^{l/2} \sum_{l''=l+l'}^{l+l'} \begin{pmatrix} l & l' & l'' \\ 0 & 0 & 0 \end{pmatrix} \begin{pmatrix} l & l' & l'' \\ -m & m & 0 \end{pmatrix} \\ \times F(\alpha z, l+l'+k+k'+2, l''), \end{aligned} \quad (18)$$

where $\begin{pmatrix} j_1 & j_2 & j_3 \\ m_1 & m_2 & m_3 \end{pmatrix}$ means the 3j symbol, and

$$\begin{aligned} F(\alpha z, l+l'+k+k'+2, l'') \\ = \int e^{-\rho} \rho^{l+l'+k+k'+2} \frac{\rho_{<}^{l''}}{\rho_{>}^{l''+1}} \rho^2 d\rho. \end{aligned} \quad (19)$$

By using the incomplete gamma function, we express the function F as

$$F(\alpha, l, l') = \frac{1}{\alpha^{l'+1}} \cdot \gamma(l+l'+1, \alpha) + \alpha^{l'} \Gamma(l-l', \alpha). \quad (20)$$

Then, we can easily evaluate these matrix elements analytically.

Thus, we determine adiabatic potentials from Equation 13, as Figure 3 shows.

Positive energy states correspond to ionized channels. So, to treat ionization processes, we included these states explicitly in the CC calculation.

Because the electron motion cannot follow the nuclear motion, we obtained the radial coupling term as

$$\langle \Psi_i | \frac{\partial}{\partial R} - \frac{1}{2} \frac{\partial}{\partial z} | \Psi_j \rangle = \sum_k \alpha_{ki} \frac{\partial}{\partial R} \alpha_{kj}. \quad (21)$$

The rotational coupling term can be simplified as

$$\langle \Psi_i | i l_y + \frac{R}{2} \frac{\partial}{\partial x} | \Psi_j \rangle = \langle \Psi_i | i l_{y'} | \Psi_j \rangle \quad (22)$$

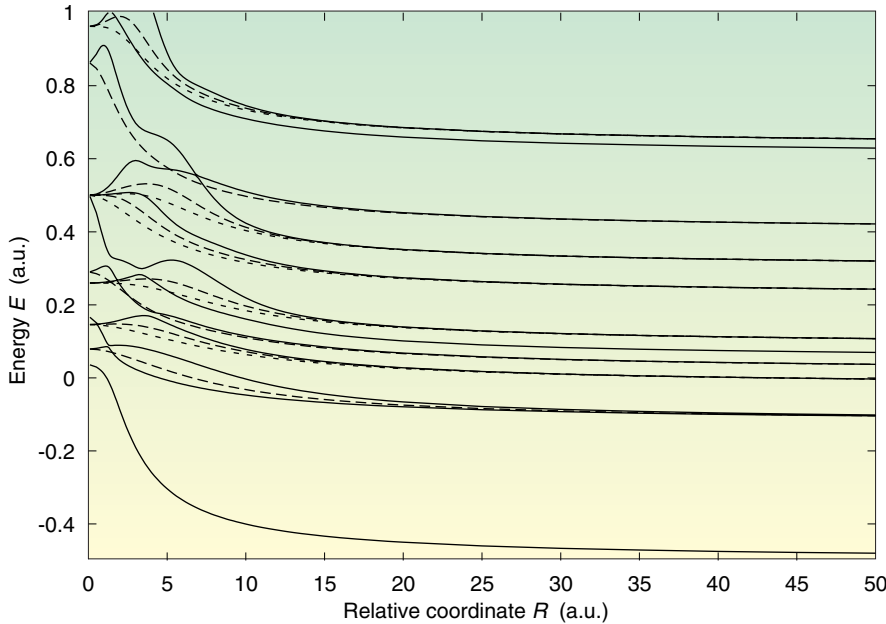


Figure 3. Adiabatic potentials of an antiprotonon–hydrogen atom system. Adiabatic potentials E below 1.0 atomic units are shown as a function of internuclear distance R . The solid lines represent Σ ($m = 0$) states, the dashed lines are Π ($m = 1$) states, and the dotted lines are Δ ($m = 2$) states. We calculated these potentials, which we determined from Equation 13 using basis function ψ_{nlm} (Equation 11, where $n \leq 5$ and $m \leq 2$). Then we got the potential energy of 31 states: 15 Σ , 10 Π , and 6 Δ .

$$\begin{aligned} & \langle \Psi_i | i l_{y'} | \Psi_j \rangle \\ &= \sum_k \sum_b \alpha_{ki} \alpha_{bj} \langle \varphi_k | -i l_{y'} | \varphi_b \rangle \end{aligned} \quad (23)$$

$$\begin{aligned} \langle \varphi_k | -i l_{y'} | \varphi_b \rangle &= \frac{1}{2} \delta_{n_k m_b} \delta_{l_k l'_b} \\ & \times \{ -\delta_{m_k m_{b+1}} \sqrt{(l_b - m_b)(l_b + m_b + 1)} \\ & + \delta_{m_k m_{b-1}} \sqrt{(l_b + m_b)(l_b - m_b + 1)} \}. \end{aligned} \quad (24)$$

Using the coupling matrix elements we evaluated and the initial condition, we solve the coupled Equation 9 using the third-order Runge-Kutta method and obtain the expansion coefficient $c_j(t)$ as a function of time.

We wrote these computer codes in Fortran 95 and calculated them in quadruple precision.

Visualization of collisions

The study of collisions through visualization has been rare, and almost no investigation for the present P-bar hydrogen–atom collision systems have been reported. Furthermore, the numerical simulation of collision processes often generates enormous amounts of data. Proper handling of these data through visualization is helpful and informative for collision dynamics studies.¹³

For this study, we calculated both the colliding particles' electron density, which changes as the collision time changes, and animated time-dependent aspects of the charge densities as a function of time.

We conducted two types of simulation studies. The first type used the electronic density of the stationary ground-state wave function as a function of the collision pair's internuclear distance. We based the second simulation on the electron density the scattering wave function obtained from the MOCC. By comparing the two simulations, we can extract the dynamical effect and highlight its significance, which permits a detailed study of the dynamics.

We conducted two types of simulation studies. The first type used the electronic density of the stationary ground-state wave function as a function of the collision pair's internuclear distance. We based the second simulation on the electron density the scattering wave function obtained from the MOCC. By comparing the two simulations, we can extract the dynamical effect and highlight its significance, which permits a detailed study of the dynamics.

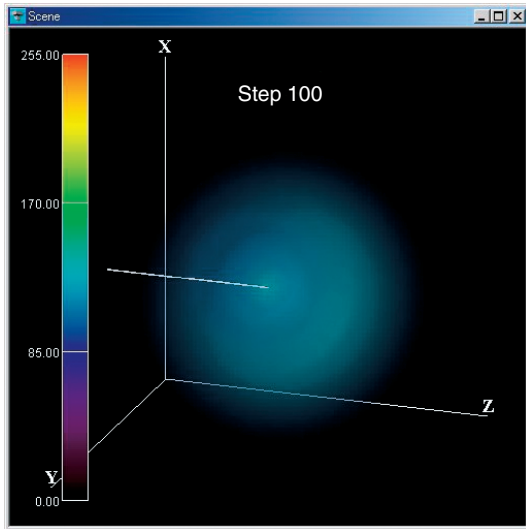


Figure 4. An example of direct volume rendering ($R = 0.11$ a.u.). The hydrogen atom's position is set at the $128 * 128 * 128$ boxels at the lattice's center. A charge density on the lattice point is normalized with a minimum value of 0 and a maximum value of 255. The discrete data's linear interpolation creates the continuous charge density map. The white line denotes an approaching antiproton. The direct-volume-rendering method enables whole-space visualization by using the semitransparency effect. First, the field data correspond with the color and semitransparency. Then, we resample the corresponding data at regular intervals with a projection of a ray, which links between viewpoints and each pixel, and is composed by finalizing the pixel's color.

Even though there are various methods that visualize 3D volume data, such as the charge density distribution, it is difficult to understand all the information using only one visualization method.¹⁴ So, we employ two different methods—direct volume rendering, which grasps the whole image easily, and interval volume rendering, which divides the image into small regions appropriate for clearly revealing the internal structure's details.^{15,16} For a phenomenon that we cannot directly observe, we can grasp the whole image at once by analyzing a huge volume of data.

We express the charge density discretely using the orthogonal and periodic lattice. For the visualization scheme, we set the hydrogen atom's position at the $128 * 128 * 128$ boxels at the lattice's center. A charge density on the lattice point is given as

$$\rho(r, t) = |\Psi(r, t; R(t))|^2 \quad (25)$$

and is normalized with a minimum value of 0 and a maximum value of 255. A continuous-charge density map is created by the discrete data's linear interpolation.

In these simulations, we adopted these conditions: the antiproton–hydrogen system's relative velocity is $v = 1.268$ atomic units (20keV), and the impact parameter \mathbf{b} is set to 0.1 a.u. (see Figure 1). At the initial starting distance of 20 a.u. from the hydrogen center for the integration, we calculated the simulation using 3,147 time steps with a time interval of 0.01 a.u.

The origin of the time, $t = 0$, is defined when an antiproton is nearest to hydrogen. We made our animations using 200 time steps from -5 a.u. to $+5$ a.u. in time.

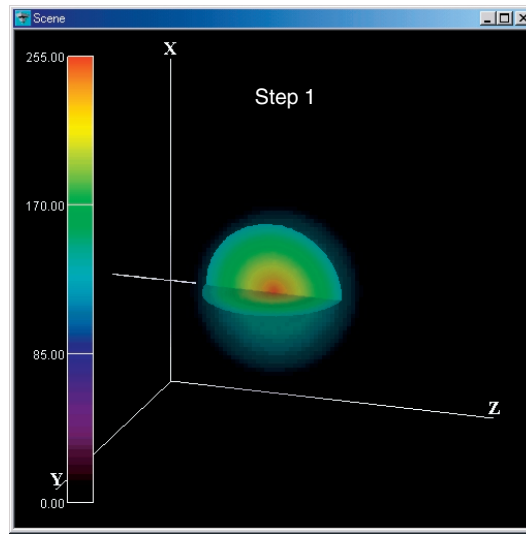
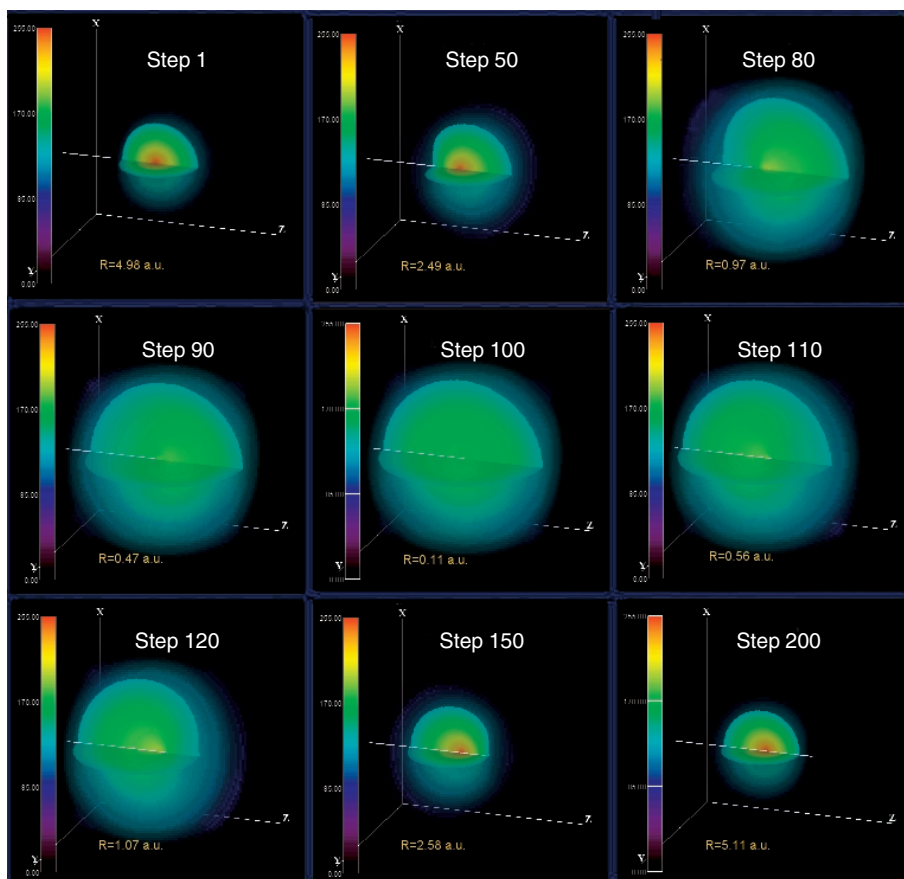


Figure 5. An example of interval volume rendering ($R = 4.98$ a.u.). The manner of display is the same as in Figure 4. Interval volume is a generalization of iso surface with a fixed value and represents a 3D subvolume for which the associated scalar values lie in a user-specified closed interval. Interval volume can be displayed as an opaque solid and can visualize the change in field values on the perimeter boundaries on the basis of the color transfer function. Coloring the cross sections lets us directly explore the volumetric region of interest's inner structure. This interval volume was set at the normalized charge density $\rho = 140 - 255$ and was cut to a quarter for a better view. On the cross section, we can see the distribution of the electron density directly. Furthermore, we covered this picture with the direct-volume-rendering figure to obtain an image consistent with the direct-volume-rendering image.

Figure 6. Nine interval-volume snapshots excerpted from an animation (animation A) of a 4D collision simulation. The antiproton (the white line) enters the visualization domain from the left and leaves to the right after the collision. R denotes the distance between the proton and antiproton. We show animation A by the static calculation results on the internuclear distance R .



To make the visualization more effectively, we used commercially available visualization software from Advanced Visual Systems and added an interval volume rendering module that Ochanomizu University's Fujishiro laboratory developed.¹⁶

By using direct volume rendering, we could visualize the whole image (see Figure 4). We showed the inner structure of the volumetric region of interest specified with interval volume rendering (see Figure 5). Furthermore, we covered this picture with the direct volume rendering figure to obtain an image consistent with the direct volume rendering image. This lets us understand the phenomenon clearly and systematically.

In Figures 6 and 7, we visualized each snapshot using interval volume rendering. We set these interval volumes between normalized $\rho = 140 - 255$ and cut to a quarter for a better view. On the cross section, we can see the electron density distribution directly.

The antiproton enters the visualization from the left and leaves to the right after the collision. The negative charge of the moving antiproton characteristically distorts the electron charge density's field around the hydrogen nucleus. As

the antiproton leaves the collision domain, the electron charge density distribution returns to its spherical shape.

To further understand the collision dynamics, we must see an electron's behavior during the collision, particularly as an antiproton comes closer to hydrogen. In ion-atom collision research, investigating how far the electron cloud spreads at each moment is important. As an antiproton approaches the target hydrogen nucleus, the discrepancy between Figure 6 (animation A) and Figure 7 (animation B) emerges clearly.

Comparing these two figures, we can clearly see the dynamical effect from step 80 to step 120. In Figure 6, the antiproton's negative charge strongly repels the electron density. However, in Figure 7, because the time of reformation is not as quick as the nucleus's relative speed, the electron density is not so widely spread.

Even after the collision, the electron cloud is still deformed by the antiproton, which is at the far right. At step 200 in Figure 7, we know the ionization takes place from the smaller radius of the electron charge density. Thus, we can easily grasp the whole collision process.

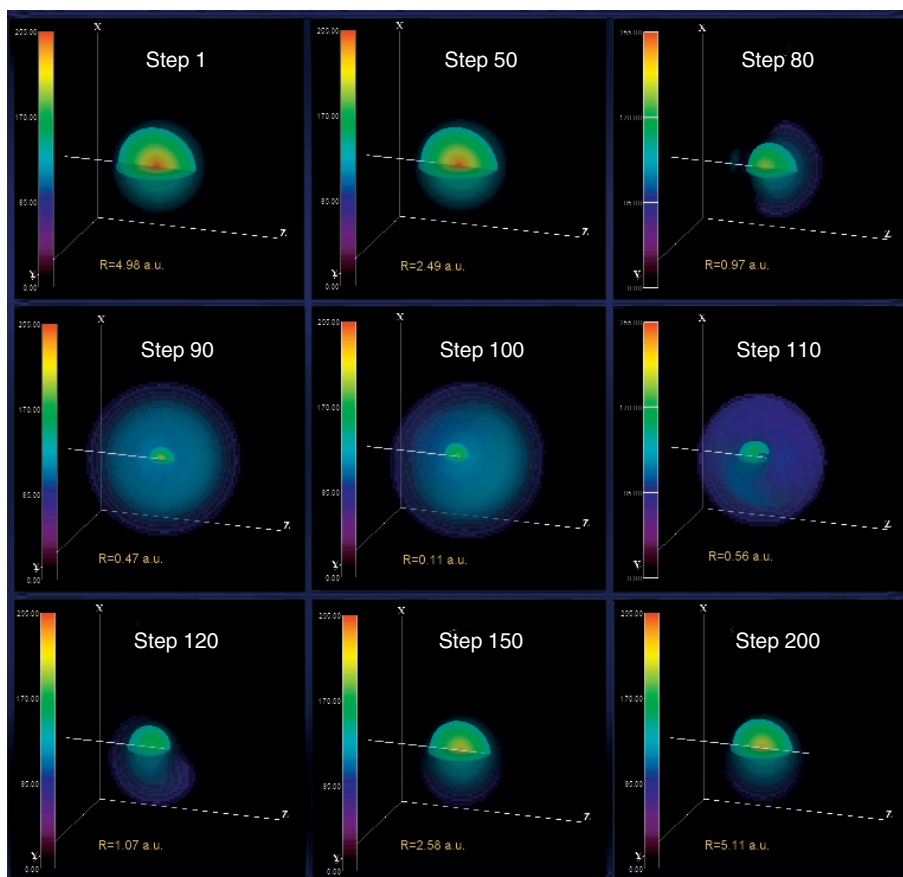


Figure 7. Nine interval-volume snapshots (animation B). We based this simulation on the electron density obtained by the scattering wave function from the molecular-orbital close-coupling. The antiproton–hydrogen system’s relative velocity is $v = 1.268$ atomic units (20 keV), and the impact parameter \mathbf{b} is set to 0.1 a.u. (see Figure 1). As an antiproton nears the target hydrogen nucleus, the discrepancy between animation A (see Figure 6) and B emerges clearly from step 80 to step 120.

Dynamical effect

To comprehend the dynamical effect, we compared the simulations based on the static picture to those of the dynamic ones. We subtracted the charge density of animation A from B at the same nuclear distance to create the animation Figure 8 shows. Red and blue volumes denote the result from animations B and A, respectively, and we rescaled the volumes to obtain a better view.

The negative charge of an antiproton deforms the ordinary electron cloud, animation A (static calculation) shows. However, for closer investigation including the dynamical effect, the electron cloud’s reformation is actually less repellent than in animation A.

Therefore, in Figure 8, the electron charge density in animation B is at first attracted to an antiproton. In animation A, however, the antiproton’s negative charge strongly repels the electron density. Therefore, we can see the red volume on the left side from step 1 to step 70.

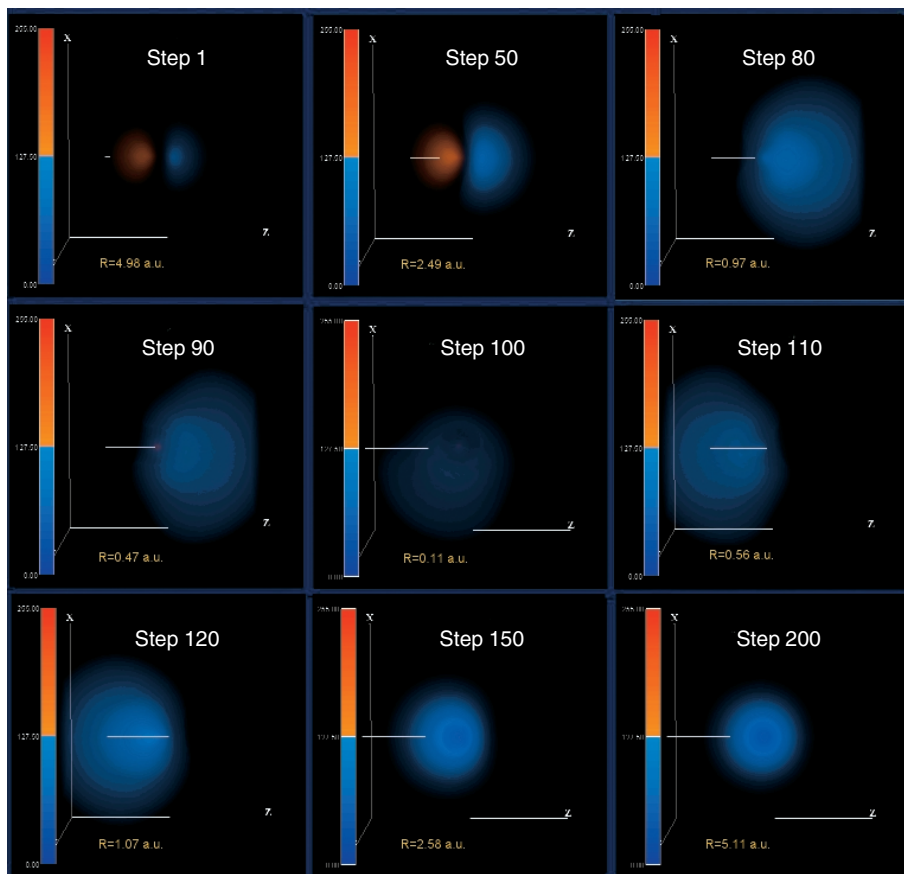
On step 200 of the dynamical figure, we know that the blue volume represents the ionized electron charge density. Thus, we can easily view the whole image of this collision process.

Clearly, the reformation of the electron cloud is less repulsive with the dynamical effect. An accurate description of electron behavior during collision is essential to better understand the dynamics and accurately determine cross sections for these processes. Through the animation, we sufficiently utilized the simulation technique to analyze the dynamics of collision processes. We investigated the collision dynamics in antiproton–hydrogen collisions at intermediate collision energies below 50 keV, using a straight-line trajectory for heavy particles. To extend the present investigation to lower collision-energy regions, we plan to conduct MOCC calculations based on a fully quantum mechanical formulation. Then, we will visualize the result using improved treatment of wave function charge density at an arbitrary point. \square

Acknowledgments

We performed this work using the interval volume rendering module, which was developed in Ochanomizu University’s Fujishiro laboratory. We acknowledge Yuriko

Figure 8. Snapshots excerpted from the simulated animation of the difference between adiabatic (animation A) and dynamical (animation B) collision simulation. We made these by subtracting the charge density of A from B at the same nuclear distance. The red and blue regions come from the dynamical results and static calculation results, respectively, and we rescaled the volumes to obtain a better view. As the red volume appears on the left side in step 1, we know the moving antiproton's effect. Because reformation of charge density is sufficient in the static calculation (blue), the electron cloud repels more from the antiproton. At step 200, we know that the blue volume represents the ionized electron charge density.



Takeshima's valuable suggestion. We thank Miho Yamauchi and Kana Yamamoto for their preliminary calculation and visualization of adiabatic state. Our work was supported in part by the Ministry of Education, Culture, Sports, Science, and Technology; the Japan Society for Promotion of Science; and the National Institute for Fusion Science in Japan.

References

1. M. Kimura and N.F. Lane, "The Low-Energy, Heavy-Particle Collisions: A Close-Coupling Treatment," *Advances in Atomic, Molecular, and Optical Physics*, vol. 26, Academic Press, San Diego, Calif., 1989, p. 79.
2. W. Fritsch and C.D. Lin, "The Semiclassical Close-Coupling Description of Atomic Collisions: Recent Developments and Results," *Physics Reports*, vol. 202, nos. 1 and 2, Apr. 1991, pp. 1–97.
3. K.A. Hall, J.F. Reading, and A.L. Ford, "Excitation and Ionization of Atomic Hydrogen by Antiprotons," *J. Physics B*, vol. 29, no. 24, 28 Dec. 1996, pp. 6123–6131.
4. J.C. Wells et al., "Numerical Solution of the Time-Dependent Schrödinger Equation for Intermediate-Energy Collisions of Antiprotons with Hydrogen," *Physical Rev. A*, vol. 54, no. 1, July 1996, pp. 593–604.
5. X. Tong et al., "Ionization of Atomic Hydrogen by Antiproton Impact: A Direct Solution of the Time-Dependent Schrödinger Equation," *Physical Rev. A*, vol. 64, no. 2, Aug. 2001, p. 22711.
6. A. Igarashi, S. Nakazaki, and A. Ohsaki, "Ionization of Atomic Hydrogen by Antiproton Impact," *Physics Rev.*, vol. 61, no. 6, May 2000, p. 62712.
7. B. Pons, "Monocentric Close-Coupling Expansion to Provide Ejected Electron Distributions for Ionization in Atomic Collisions," *Physical Rev. Letters*, vol. 84, no. 20, May 2000, pp. 4569–4572.
8. K. Sakimoto, "A Theoretical Study of Ionization Processes in Low-Energy Collisions between Antiprotons and Atomic Hydrogen Using Discrete-Variable-Representation Methods," *J. Physics B*, vol. 33, no. 16, 28 Aug. 2000, pp. 3149–3164.
9. N. Toshima, "Two- and One-Center Close-Coupling Calculations for Ionization of Atomic Hydrogen by Antiproton Impact," *Physical Rev. A*, vol. 64, no. 2, Aug. 2001, p. 24701.
10. H. Knudsen et al., "Ionization of Atomic Hydrogen by 30-1000 keV Antiprotons," *Physical Rev. Letters*, vol. 74, no. 23, 5 June 1995, pp. 4627–4630.
11. A. Watanabe et al., "Calculation of Non-Adiabatic Coupling Matrix Elements in the Molecular Orbital Expansion Method," *Natural Science Report of the Ochanomizu Univ.*, vol. 49, no. 2, Dec. 1998.
12. B.H. Bransden and C.J. Joachain, *Physics of Atoms and Molecules*, Longman, New York, 1983, pp. 128–154.
13. A. Watanabe et al., "Visualization of Proton-Hydrogen Atom Collision at Low and Intermediate Energy," *J. Visualization Soc. Japan*, vol. 18, no. 68, Jan. 1998, pp. 23–28.
14. A.E. Kaufman, *Volume Visualization*, IEEE CS Press, Los Alamitos, Calif., 1991.

15. I. Fujishiro, Y. Maeda, and H. Sato, "Interval Volume: A Solid Fitting Technique for Volumetric Data Display and Analysis," *Proc. 6th IEEE Visualization Conf. (Visualization 95)*, IEEE CS Press, Los Alamitos, Calif., 1995, pp. 151-158.
16. I. Fujishiro et al., "Volumetric Data Exploration Using Interval Volume," *IEEE Trans. Visualization and Computer Graphics*, vol. 2, no. 2, June 1996, pp. 144-155.

Reiko Suzuki is a research assistant at the Computer Center at Hitotsubashi University. Her research interests include atomic-collision physics and scientific visualization. She received her MSc from Ochanomizu University, Tokyo. She is a member of the Information Processing Society and the Physical Society of Japan. Contact her at the Computer Ctr., Hitotsubashi Univ., 2-1 Naka, Kunitachi, Tokyo 186-8603, Japan; susuki@cc.hit-u.ac.jp.

Hiroshi Sato is an information sciences professor at Ochanomizu University. His research interests include atomic-collision physics and scientific visualization. He received his MSc at the Tokyo Institute of Technology and his DSc at Waseda University, Tokyo. He is a member of the Information Processing Society of Japan, the Visualization Society of Japan, the Physical Society of Japan, and the Society for Atomic Collision Research. Contact him at the Dept. of Information Sciences, Ochanomizu Univ., 2-1-1 Otsuka, Bunkyo-Ku, Tokyo 112-8610, Japan; sato@is.ocha.ac.jp.

Mineo Kimura is a physics professor at the Graduate School of Science and Engineering at Yamaguchi University. His research interests include atomic and molecular physics, chemical physics, medical physics, radiation physics, chemistry and biology, condensed-matter physics and chemistry, biophysics, biochemistry, and computer science. He has an MSc from Waseda University and a PhD from the University of Alberta. He is a member of the American Physical Society, the Radiation Research Society, and the Sigma Xi Honor Society. Contact him at the Graduate School of Science and Eng., Yamaguchi Univ., Ube, Yamaguchi 755-8611, Japan; mineo@po.cc.yamaguchi-u.ac.jp.

For more information on this or any other computing topic, please visit our Digital Library at <http://computer.org/publications/dlib>.

Member Societies

American Physical Society
Optical Society of America
Acoustical Society of America
The Society of Rheology
American Association of Physics Teachers
American Crystallographic Association
American Astronomical Society
American Association of Physicists in Medicine
AVS
American Geophysical Union
Other Member Organizations
Sigma Pi Sigma, Physics Honor Society
Society of Physics Students
Corporate Associates

The American Institute of Physics is a not-for-profit membership corporation chartered in New York State in 1931 for the purpose of promoting the advancement and diffusion of the knowledge of physics and its application to human welfare. Leading societies in the fields of physics, astronomy, and related sciences are its members.

The Institute publishes its own scientific journals as well as those of its Member Societies; provides abstracting and indexing services; provides online database services; disseminates reliable information on physics to the public; collects and analyzes statistics on the profession and on physics education; encourages and assists in the documentation and study of the history and philosophy of physics; cooperates with other organizations on educational projects at all levels; and collects and analyzes information on Federal programs and budgets.

The scientists represented by the Institute through its Member Societies number approximately 120,000. In addition, approximately 5,400 students in over 600 colleges and universities are members of the Institute's Society of Physics Students, which includes the honor society Sigma Pi Sigma. Industry is represented through 47 Corporate Associates members.

Governing Board*

John A. Armstrong, (Chair), *Marc H. Brodsky* (Executive Director), *Benjamin B. Snavely* (Secretary), Martin Blume (APS), William F. I. Brinkman (APS), Judy R. Franz (APS), Donald R. Hamann (APS), Myriam P. Sarachik (APS), *Thomas J. McIlrath* (APS), George H. Trilling (APS), *Michael D. Duncan* (OSA), Ivan P. Kaminow (OSA), Anthony M. Johnson (OSA), Elizabeth A. Rogan (OSA), Anthony A. Atchley (ASA), *Lawrence A. Crum* (ASA), Charles E. Schmid (ASA), Arthur B. Metzner (SOR), Christopher J. Chiaverina (AAPT), Charles H. Holbrow (AAPT), John Hubisz (AAPT), *Bernard V. Khoury* (AAPT), Charlotte Lowe-Ma (ACA), S. Narasinga Rao (ACA), Leonard V. Kuhl (AAS), Arlo U. Landolt (AAS), Robert W. Milkey (AAS), *James B. Smathers* (AAPM), Christopher H. Marshall (AAPM), *Rudolf Ludeke* (AVS), N. Rey Whetten (AVS), Dawn A. Bonnell (AVS), James L. Burch (AGU), Robert E. Dickinson (AGU), Jeffrey J. Park (AGU), Judy C. Holoviak (AGU), *Louis J. Lanzerotti* (AGU), Fred Spilhaus (AGU), Brian Clark (2002) MAL, Frank L. Huband (MAL)

*Executive Committee members are printed in italics.

Management Committee

Marc H. Brodsky, Executive Director and CEO; Richard Baccante, Treasurer and CFO; Theresa C. Braun, Vice President, Human Resources; James H. Stith, Vice President, Physics Resources; Darlene A. Walters, Senior Vice President, Publishing; Benjamin B. Snavely, Secretary

Subscriber Services

AIP subscriptions, renewals, address changes, and single-copy orders should be addressed to Circulation and Fulfillment Division, American Institute of Physics, 1NO1, 2 Huntington Quadrangle, Melville, NY 11747-4502. Tel. (800) 344-6902; e-mail subs@aip.org. Allow at least six weeks' advance notice. For address changes please send both old and new addresses, and, if possible, include an address label from the mailing wrapper of a recent issue.